Journal of South American Earth Sciences 106 (2021) 103051

Contents lists available at ScienceDirect

Journal of South American Earth Sciences

journal homepage: www.elsevier.com/locate/jsames

South Atlantic passive margin evolution: A thermochronology case study from the Rio de Janeiro-Três Rios section, SE Brazil

J.N. Gezatt [a,*], D.I.M. Macdonald [a], R. Stephenson [a], A.R. Jelinek [b], A. Carter [c]

[a] Department of Geology and Geophysics, University of Aberdeen, King's College, Aberdeen, AB24 3UE, UK
[b] Departamento de Geodésia, Instituto de Geociências, Universidade Federal do Rio Grande do Sul, Av. Bento Gonçalves, 9500, Porto Alegre, Rio Grande do Sul, CEP 90650-970, Brazil
[c] Department of Earth and Planetary Sciences, Birkbeck College, Malet Street, London, WC1E 7HX, UK

ARTICLE INFO

Keywords:
Fission track
(U–Th)/He
Passive margin
Thermal history modelling
Southeastern Brazil
Thermochronology

ABSTRACT

The southeastern Brazilian passive margin records a complex post-rift evolution, with two parallel high-elevation features formed after the opening of the South Atlantic. We applied apatite fission track (AFT) and U–Th/He (AHe) low temperature thermochronology to constrain the thermo-tectonic history of the Serra do Mar escarpment in the area of Rio de Janeiro state. New AFT central ages for basement areas collected from a N–S transect orthogonal to the shoreline between the cities of Rio de Janeiro and Três Rios, range between 98.5 ± 5.3 and 54.1 ± 4.2 Ma, with mean track lengths between 12.34 ± 0.40 and 14.63 ± 0.17 μm. Uncorrected AHe ages lie between 68.1 ± 5.9 and 60.2 ± 7.3 Ma and are consistent with AFT results. Inverse thermal history models constrained by AFT and AHe data imply the earliest cooling onset from the Barremian (Early Cretaceous), with steady rates more common for samples closer to coastal areas. Maximum depths of denudation are between 2.5 and 4.5 km. Published thermochronological data from adjacent areas combined with the new results show a seemingly simpler post-rift evolution for the area, although suggesting structural control of age distribution and exhumation.

1. Introduction

Passive continental margins yield a valuable record of continental rifting as well as of other lithosphere and mantle dynamic processes. Rifted margin escarpments are significant geomorphological features that separate elevated regional-scale plateaus from neighbouring low-lying coastal plains on a number of continental passive margins around the world, known as high-elevation rifted margins (Gilchrist and Summerfield 1990). There is considerable debate on whether these features were inherited from the rifting process or earlier orogenic events, or if they reflect post-rift tectonic reactivation (Gallagher et al., 1994; Brown et al., 2002; Nielsen et al., 2009; Japsen et al., 2012; Blenkinsop and Moore 2013; Jelinek et al., 2014).

The Atlantic rifted margins represent a particularly complex puzzle, especially given their significant geographical extent and assemblage of geological features. The Brazilian passive margin, topographically and bathymetrically distinct from its African conjugate (Gallagher and Brown 1997; Aslanian et al., 2009), can be divided into at least two segments with distinct rifting responses during the Jurassic-Cretaceous opening of the South Atlantic Ocean (Chang et al., 1992; Heine et al., 2013; Brune et al., 2018). The Equatorial segment developed in response to transform motion between the continental plates, while the remainder of the passive margin, further south, evolved from oblique to orthogonal extension. Specifically, the modern coastline in the south-eastern segment of the Brazilian margin is subparallel to the main NE-SW Precambrian structures, as the propagation of the rift system seems to have followed major pre-existing Brasiliano-Pan-African structures (Tommasi and Vauchez, 2001; Buiter and Torsvik, 2014; Schmitt et al., 2016). Continental breakup in the area took place around 130 Ma (Chang et al., 1992; Macdonald et al., 2003). Fig. 1 shows the tectonic setting of the southeastern segment of the Brazilian continental margin and the location of the present study.

The southeastern portion of the Brazilian continental margin contains two escarpments parallel to the shoreline that reach up to 2000 m above sea level: the Serra da Mantiqueira, farthest inland, and the Serra do Mar, closer to the coast, separated from the continental shelf onshore of the marginal Santos Basin by a narrow coastal plain (Figs. 1 and 2). The study of the present-day regional landscape can constrain the

* Corresponding author.
E-mail address: gezatt@abdn.ac.uk (J.N. Gezatt).

https://doi.org/10.1016/j.jsames.2020.103051
Received 9 June 2020; Received in revised form 29 September 2020; Accepted 18 November 2020
Available online 24 November 2020

formation of the high elevation features and help unveil the evolution of the rifted margin and its contribution to the sedimentary input of the offshore adjacent basins (Karner and Driscoll 1999; Milani et al., 2001; Macdonald et al., 2003).

Low-temperature thermochronology is an ideal tool to investigate upper crust thermal and erosional histories, as it records the effect of cooling and heating episodes within the shallow crust that can, in turn, reflect regional geodynamic processes and their surface development. Apatite fission track analysis (AFT) is sensitive to temperatures between 120 °C and 60 °C (Gleadow et al., 1986; Wagner et al., 1989; Donelick et al., 2005) and apatite U–Th/He dating (AHe), to temperatures between ~120 °C and 40 °C (Farley, 2000; Flowers et al., 2009; Gautheron et al., 2009; Ault et al., 2019). The application of these methods can help indicate if the high topography features are remnant of rifting or if there is a thermal record of post-rift tectonic activity (Brown et al., 1990; Gallagher et al., 1994; O'Sullivan et al., 2000; McGregor et al., 2013; Wildman et al. 2015, 2019).

This study provides new regional constraints to the post-rift thermal evolution of the Rio de Janeiro-Três Rios segment of the SE Brazilian continental margin from AFT and AHe analysis (Fig. 2). Whilst the Brazilian rifted margin has been the subject of previous thermochronological investigations, there is a data gap in the margin section in the state of Rio de Janeiro and, hence, the understanding of the rifted margin in the SE of Brazil is incomplete. To address this we collected a strategic suit of samples across this previously unstudied segment of the continental margin for apatite thermochronology. The resulting data will help to provide a more complete margin-wide comprehension of the geodynamic mechanisms responsible for the present-day topography in the area. We present cooling ages as well as evidence of steady cooling after the breakup of SW Gondwana and, coupled with previously published regional low-temperature data, point out potential geological controls for the uplift process that led to the formation of the Serra do Mar escarpment in the state of Rio de Janeiro, comparing it to other segments of the SE Brazilian continental margin.

2. Geological setting

The lithologies that occur throughout the present-day SE Brazilian passive margin were dominantly formed by the Neoproterozoic-Cambrian tectonic events that led to the consolidation of Western Gondwana during the Brasiliano-Pan-African Orogenic Cycle (Brito Neves and Cordani 1991; Schmitt et al., 2008; Brito Neves et al., 2014). This long-lived convergence event resulted in a complex NE-SW-striking structural framework formed by high angle strike-slip shear zones (Ebert and Hasui 1998; Trouw et al., 2000) that comprises syn-to post-orogenic medium-to high-grade metamorphic rocks and associated magmatic intrusions (Heilbron et al. 2008, 2020). The Ribeira Fold Belt Precambrian-Cambrian terranes are overlain by the sediments of the Ordovician-Cretaceous cratonic Paraná Basin to the west (Fig. 1). The Cretaceous volcanic rocks of the Serra Geral Formation, the Brazilian continental portion of the Paraná-Etendeka Large Igneous Province, have been dated at 134.6 ± 0.6 Ma by bulk-rock Ar–Ar and zircon/-baddeleyite U–Pb (Thiede and Vasconcelos 2010 and references therein; Janasi et al., 2011, respectively). Unconformably lying on Late Jurassic rift stage aeolian strata, the flood basalts and acid volcanic rocks were extruded synchronously with the opening of the South Atlantic and can

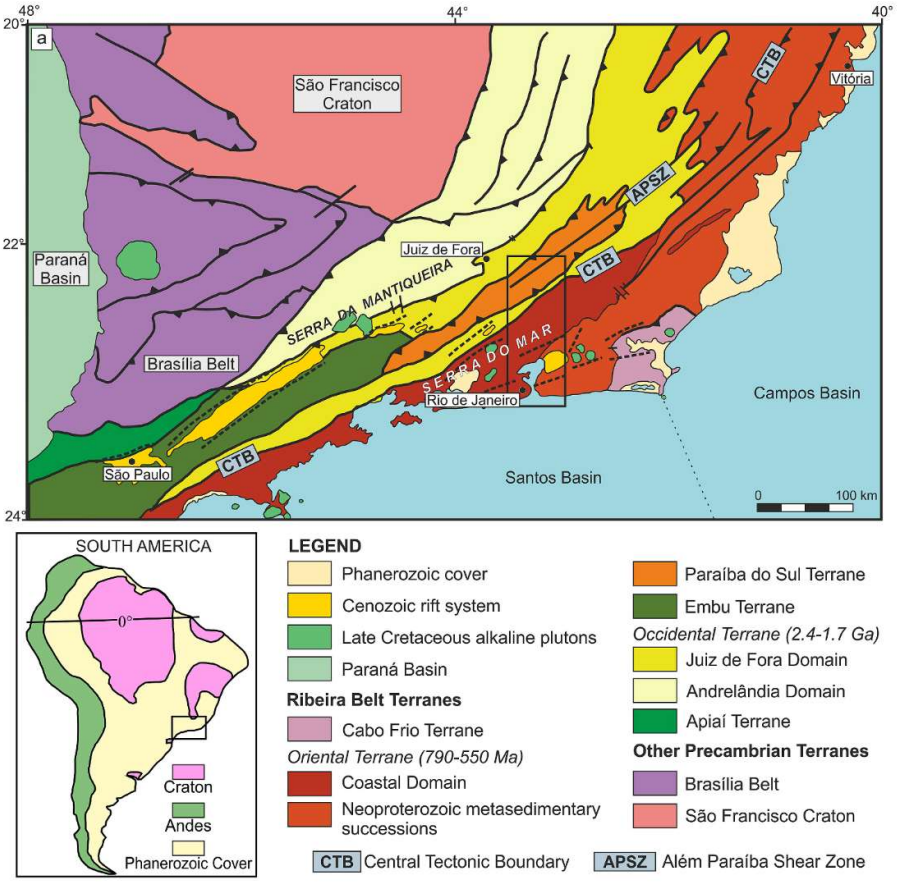

Fig. 1. Geotectonic map of the SE rifted margin in Brazil (after Heilbron et al., 2008). The black dashed lines outline the Cenozoic rift system onshore structural framework. The black box outlines the location of the study area of this work. Refer to text for detail on the regional geology.

be correlated to the basement of the marginal Santos, Campos and Espírito Santos basins (Thomaz Filho et al., 2008; Stica et al., 2014).

The marginal Santos and Campos basins started to develop prior to the opening of the South Atlantic (Chang et al., 1992) and have well known structural frameworks and stratigraphy as a consequence of extensive surveying for hydrocarbon exploration (e.g. Mohriak et al., 1990; Cainelli and Mohriak 1999; Modica and Brush 2004; Contreras et al., 2010; Stanton et al., 2010; Beglinger et al., 2012; Pichel et al., 2019). The main transitional to post breakup source areas of siliciclastic sediments for these basins have been the Serra do Mar, and later, the Serra da Mantiqueira escarpments, with sediment transportation and feeding happening mainly through the Paraíba do Sul River (Cobbold et al., 2001; Zalán and Oliveira 2005).

Onshore post breakup magmatism took place between ca. 85 and 55 Ma (Almeida et al., 1996; Geraldes et al., 2013), emplacing alkaline intrusions such as the Poços de Caldas and Itatiaia complexes, positioned along what Almeida (1991) named the Cabo Frio Lineament. Thompson et al. (1998) attributed the alkaline magmatism to the eastward drift of the South American plate over the Trindade hot spot. Riccomini et al. (2005), on the other hand, argued that radiometric ages of the alkaline bodies did not show linear progress eastward and that their emplacement was a consequence of the regional structural framework, where a

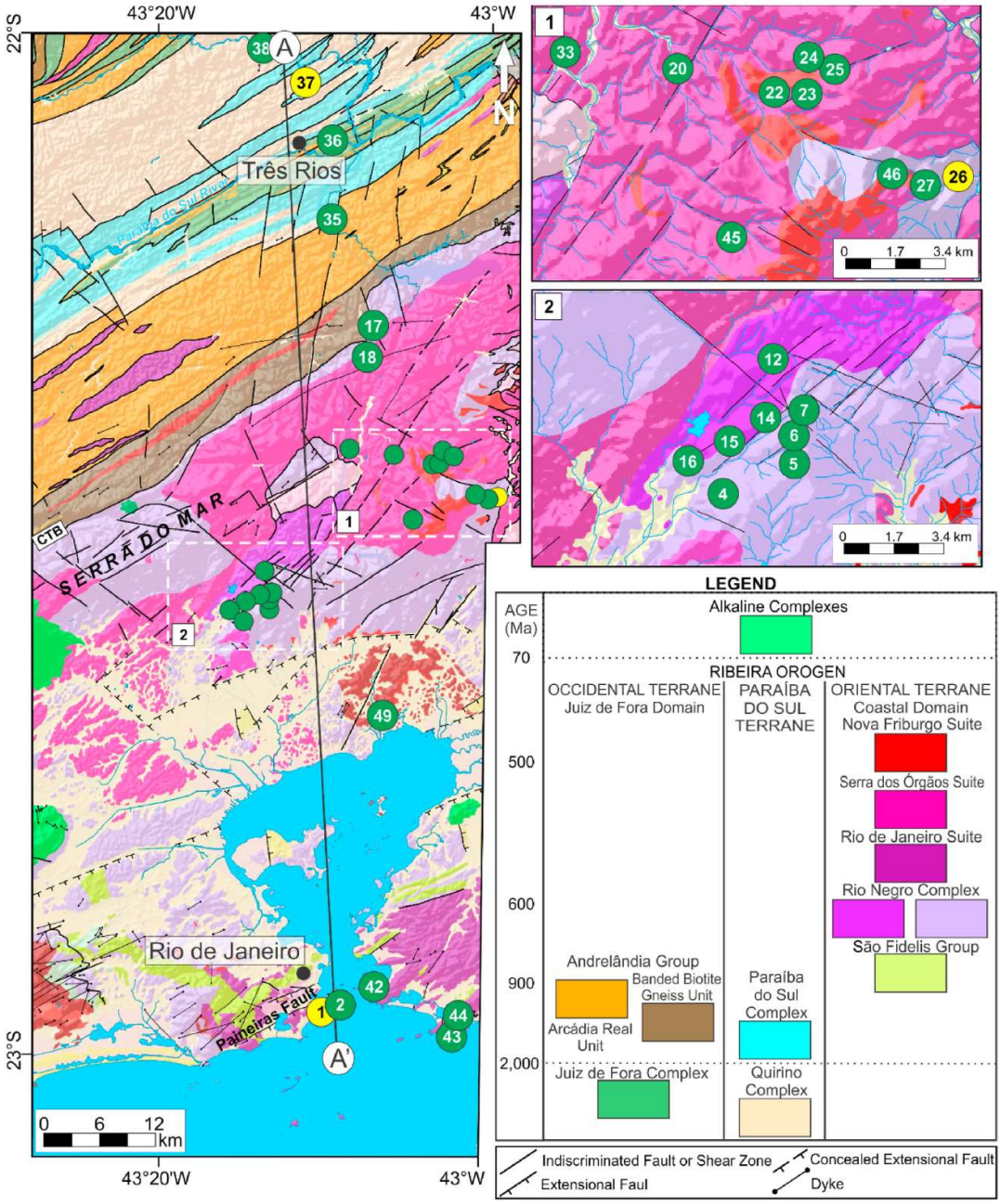

Fig. 2. Sample locations in the study area (for location of the geological map see Fig. 1). CTB is the Central Tectonic Boundary. Geological map from CPRM (2009a, b). Location of the Paineiras Fault after Ferrari (2001). Samples undergone AFT analysis are labelled in green, while yellow labels indicate those samples analysed with both AFT and AHe methods. (For interpretation of the references to colour in this figure legend, the reader is referred to the Web version of this article.)

fracture zone was under the influence of a WNW-ESE-oriented strain.

Cenozoic basin formation occurred onshore the Santos Basin after the separation of the Serra do Mar and Serra da Mantiqueira escarpments as a consequence of structural reactivation (Sacek et al., 2012; Cogné et al., 2013; Franco-Magalhaes et al., 2014; Vieira and Gramani, 2015), during a series of deformation phases. These processes originated structure-embedded SW-NE to E-W-trending rift basins such as São Paulo, Taubaté, Resende and Guanabara which, among other basins, form the Cenozoic Continental Rift of Southeast Brazil (Riccomini et al., 2004). Zalán and Oliveira (2005) identified the offshore associated rifts using gravimetric and magnetic data, and named it the Cenozoic Rift System of Southeastern Brazil as opposed to a single rift, incorporating the different rift basins.

3. Materials and methods

Thirty Precambrian basement outcrop samples were collected in a N–S transect between the cities of Rio de Janeiro and Três Rios in the Brazilian state of Rio de Janeiro, orthogonal to the modern shoreline and approximately so to major structural trend. Sampling was generally done on road cut outcrops observing a desired 100 m vertical distance between sample locations, aiming to obtain a fairly representative sampling grid of the vertical age distribution along the profile. In total, 49 sites were sampled, while 30 of these had samples analysed by AFT, as the remaining samples yielded very few or no apatite crystals, or revealed very low uranium concentrations and did not allow track counting.

3.1. Apatite fission track

Analysis was performed in the London Geochronology Centre at UCL/Birkbeck. Apatite crystals were separated from ~5-kg samples using standard crushing, sieving, magnetic, and heavy liquid procedures, and embedded in epoxy resin for fission track analysis. The polished grains were then treated with 5.0 M HNO_3 for 20 s at 21 °C to reveal spontaneous tracks (Hurford 1990). Following attachment of a low-U mica external detector (Gleadow 1981; Hurford and Green 1982), Durango and Fish Canyon Tuff apatite standards, and CN5 dosimeter glasses, samples were irradiated in the Forschungsneutronenquelle Heinz Maier–Leibnitz (FRM II) reactor at Technical University of Munich. Induced tracks in the mica detectors were etched with 48% HF during 18 min at 20 °C.

Spontaneous track count was done for 20 grains per sample (when available) using a zeta (ζ) calibration (Hurford 1990) value of 338.5 ± 5.0 for CN5 dosimeter. Samples were counted using a Zeiss Axioplan microscope with total magnification of 1250x. For confined track and etch pit diameter (Dpar) measurements (Donelick et al., 2005) a coupled Kinetek XY stage and digitalising tablet was used under computer control. Confined track lengths were measured for 100 tracks depending on abundance. Chlorine wt% was done for 15 of the samples and measured using a Microscan MK5 electron microprobe with a 5 μm beam at an acceleration voltage of 15 keV and 6.0 nA current at the University of Aberdeen. AFT results are reported as central ages (Galbraith 1992) and uncertainties are for 1σ standard error.

3.2. Apatite U–Th/He

Given that the AFT age data were closely similar, AHe analyses were obtained from 3 samples that represented the sample location, elevation and AFT age range. As the results recorded effectively the same thermal histories no further AHe analyses were required. Analysis was performed in the London Geochronology Centre at UCL/Birkbeck. Four to six euhedral inclusion- and fracture-free grains were analysed per sample. Grains were hand-picked using a binocular microscope and selected grains further assessed under higher magnification using a Zeiss Axioplan microscope at a magnification of 1250x. Individual grains packed into a platinum tube were heated with an 808 nm iodine laser beam to 900–1000 °C for 60 s, in order to degas the crystal for ^{4}He measurement using a Pfeiffer Prisma 100 with Quadstar QS422 software. Gas volumes were determined by isotope dilution using two 5800 cc vacuum tanks with gas pipettes for delivering known aliquots of helium. The ^{4}He Standard Tank (Q Tank), pipette volume 0.3222 cc contains isotopically pure ^{4}He that is used as the gas standard against which samples and blanks are determined. The ^{3}He Spike Tank, pipette volume 0.2258 cc contains isotopically pure ^{3}He and is used for isotope dilution of samples and blanks.

Following extraction, the Pt tubes were removed and placed in vials for dissolution. Tube ends were prised open to ensure solutions could get into the tube and dissolve the apatite grain. A 30 μl spike with a known concentration of ^{235}U, ^{230}Th and ^{149}Sm, which included HNO_3, was added to each vial and left for 24 h at room temperature, enough to dissolve apatite grains. After this, vials were topped up with 1500 μl of water ready for measurement on an Agilent 7700x ICP-MS. Each solution run included spike, acid and water blanks plus Durango age standards. Spike solutions were re-calibrated for each session. Errors on ages use the reproducibility of the Durango age standard which at the time of analysis was 7%.

3.3. Inverse thermal modelling

Apatite thermal history models were done with software QTQt (Gallagher 2012) which uses a transdimensional Markov Chain Monte Carlo (MCMC) inversion to sample from possible thermal histories (Gallagher 1995) and build a spectrum of models which probabilistically fit the thermal data input. Modelling was carried out for 22 samples with more than 50 confined track length measurements using multi-kinetic annealing model from Ketcham et al. (2007) and using track lengths projected against their orientation to the crystallographic c-axis. Samples with AHe analysis were modelled using the Flowers et al. (2009) radiation damage model with spherical geometry diffusion. The model choice was based on the protracted cooling obtained during exploratory runs as well as on the time of residency in the He partial retention zone (HePRZ). Input data contained individual sample track density counts, composition values (Dpar measurements or Cl wt% when available), confined track measurements and respective angle to c-axis, and zeta parameter value. In the absence of geological constraints, forward models were used to test various scenarios such as samples being at or close to the surface and then reburied or simple exhumation from depth. As these runs also defined the oldest tracks (the approximate point at which the AFT data cannot constrain older thermal histories), it was decided to use a t-T constraint of 130 ± 10 Ma and 120 ± 10 °C, corresponding to the South Atlantic rifting. Surface temperature was set at 20 ± 10 °C.

Models were run for 500 thousand iterations and are reproduced here as an expected curve (the mean thermal history curve weighted for its posterior probability) with 95% associated credible intervals. Samples JG-01, JG-26 and RJ-37 were modelled with both AFT and AHe data.

4. Results

4.1. Apatite fission track data

AFT central ages range between 98.5 ± 5.3 and 54.1 ± 4.2 Ma, with sampling heights lying between 0 and 1541 m above sea level (Table 1). Younger ages are found towards the coast, and become progressively older towards the continental interior, with older ages also found at higher elevations (Fig. 3). Measured mean confined track lengths (MTL) vary between 12.34 and 13.89 μm, while c-axis corrected MTL range between 13.51 and 15.21 μm, and distributions are predominantly unimodal. Mean Dpar values range from 1.52 to 4.10 μm, illustrating compositional variation between samples. Sample J-49 has the highest

Table 1
Summary of apatite fission track data.

Sample	Lat	Long	Elev.	No of	Dosimeter		Spontaneous		Induced		Age dispersion		Central Age	±1σ	Mean Cl wt	MTL	S.D.	n	Mean Dpar
			(m)	crystals	ρ_d	N_d	ρ_s	N_s	ρ_i	N_i	$P\chi^2$	RE%	(Ma)	(Ma)	%	(μm)	(μm)		(μm)
JG-1	−22.94	−43.16	0	20	1.687	4676	1.169	1369	4.689	5542	30.7	5.0	70.1	2.5	0.01	13.10	1.4	75	1.5
JG-2	−22.94	−43.15	16	20	1.687	4676	0.227	205	1.172	1075	99.1	0.0	54.1	4.2	0.01	–	–	–	–
JG-4	−22.56	−43.26	287	20	1.687	4676	0.384	185	1.593	781	94.8	0.0	67.2	5.6	0.002	–	–	–	–
RJ-5	−22.55	−43.22	612	20	1.819	5042	0.481	324	1.574	1126	31.8	3.4	87.9	5.7	–	12.83	1.6	49	2.6
RJ-6	−22.54	−43.22	768	20	1.819	5042	0.596	382	2.087	1345	25.9	4.3	86.9	5.3	–	–	–	–	2.3
RJ-7	−22.53	−43.22	812	20	1.819	5042	0.859	6.5	3.112	2223	67.9	0.4	83.1	4.0	–	12.94	1.6	90	2.4
JG-12	−22.51	−43.23	774	20	1.687	4676	0.765	456	2.98	1791	79.9	0.0	72.2	3.9	0.000	13.08	1.2	100	2.1
JG-14	−22.53	−43.24	444	20	1.687	4676	0.887	514	3.431	2031	15.16	9.4	72.4	4.1	0.001	13.59	1.5	105	2.2
RJ-15	−22.54	−43.25	318	20	1.819	5042	0.541	379	2.486	1691	68.5	4.0	68.5	4.1	–	12.34	1.7	19	1.8
JG-16	−22.55	−43.27	178	20	1.687	4676	1.097	742	4.358	3014	31.05	8.5	70.3	3.4	0.06	12.57	1.5	102	1.9
JG-17	−22.28	−43.13	663	19	1.687	4676	1.086	567	3.76	1955	84.2	0.0	82.2	4.1	0.017	13.55	1.6	83	3.5
JG-18	−22.30	−43.13	706	17	1.687	4676	1.856	992	6.887	3611	33.5	1.2	77.8	3.0	0.01	13.19	1.4	90	1.6
JG-20	−22.40	−43.10	740	30	1.687	4676	0.207	251	0.666	828	94.2	0.2	85.9	6.3	0.008	–	–	–	1.7
JG-22	−22.41	−43.06	1155	22	1.687	4676	0.314	214	1.108	837	5.2	24.3	75.0	7.1	0.005	13.71	1.3	3	1.6
JG-23A	−22.41	−43.05	1216	21	1.687	4676	0.725	300	2.797	1198	27.7	14.9	71.3	5.3	0.002	13.89	1.1	55	1.8
RJ-24	−22.40	−43.05	1303	20	1.819	5042	0.57	337	2.111	1285	29.2	5.8	80.3	5.2	–	13.18	1.3	100	2.4
RJ-25	−22.40	−43.04	1436	20	1.819	5042	0.947	692	3.23	2390	58.4	0.4	88.4	4.0	–	12.81	1.0	100	2.4
JG-26	−22.44	−43.00	1179	20	1.687	4676	0.75	456	2.512	1543	39.4	7.1	83.7	4.8	0.0004	13.59	1.3	103	2.0
JG-27	−22.44	−42.99	1043	20	1.687	4676	0.919	511	3.073	1709	59.4	0.2	84.7	4.4	0.017	13.34	1.4	110	1.7
RJ-33	−22.40	−43.14	751	20	1.819	5042	1.073	674	3.999	2517	67.2	0.3	81.8	3.7	–	12.94	1.3	100	1.9
JG-35	−22.17	−43.17	297	20	1.687	4676	0.802	816	1.687	2727	30.8	4.9	84.8	3.7	0.044	13.33	1.3	100	1.7
RJ-36	−22.10	−43.17	291	20	1.819	5042	1.231	1017	4.046	3415	0.6	14.6	91.3	4.7	–	13.15	1.4	100	2.0
RJ-37	−22.04	−43.20	330	20	1.819	5042	1.058	1078	3.426	3462	32.3	0.4	95.0	3.6	–	12.99	1.7	70	2.3
JG-38	−22.01	−43.24	314	20	1.687	4676	0.135	232	0.56	966	94.9	0.0	68.1	5.1	0.006	–	–	–	–
J-42	−22.92	−43.12	6	20	1.762	4784	0.94	930	3.703	3681	56.2	0.8	74.8	3.0	–	13.90	1.6	77	2.5
J-43	−22.97	−43.03	4	20	1.762	4784	1.562	955	5.72	3598	19.4	4.6	78.8	3.2	–	13.83	1.4	94	3.1
J-44	−22.95	−43.02	134	20	1.762	4784	1.161	931	4.201	3425	23.3	5.2	80.5	3.3	–	13.56	1.5	109	2.5
J-45	−22.46	−43.08	1541	20	1.762	4784	0.527	685	1.588	2055	8.2	11.9	98.5	5.3	–	14.63	1.4	71	3.6
J-46	−22.43	−43.01	1513	20	1.762	4784	0.406	386	1.216	1199	6.2	18.6	96.1	7.1	–	13.90	1.6	20	2.4
J-49	−22.66	−43.11	16	20	1.762	4784	0.871	819	3.034	2832	19.1	8.0	85.5	3.9	–	13.93	1.3	103	4.1

Track densities are (x10^6 tr cm^{-2}); analyses by external detector method using 0.5 for the 4π/2π geometry correction factor; central age is a modal age, weighted for different precisions of individual crystals (Galbraith, 1992); ρ_s: measured spontaneous track density; N_s: number of spontaneous tracks counted; ρ_i: measured induced track density; N_i: number of induced tracks counted; ρ_d: track density measured in glass dosimeter; N_d: number of tracks counted in determining ρ_d; 1σ: standard deviation; χ^2: Chi-square probability; n: number of confined tracks lengths measured; MTL: mean track length; Dpar: mean etch pit diameter of all measured etch pits; S.D.: standard deviation of track length distribution of individual track measurements; (−): not analysed. Note: AFT ages were calculated by Prof. A. Carter using ζ CN5 = 338.5 calibrated by multiple analyses of IUGS apatite and zircon age standards (Hurford, 1990). Coordinate datum WGS 84.

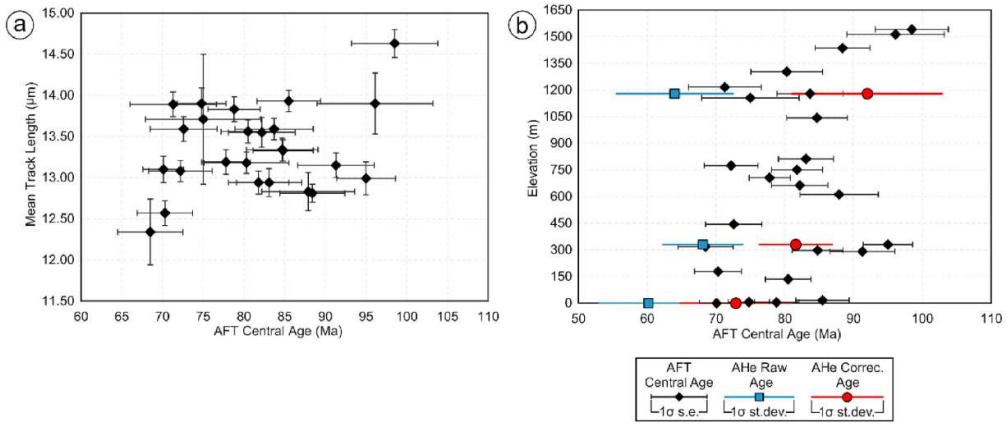

Fig. 3. AFT age distribution. (a) Relationship between AFT central ages and measured MTL – boomerang plot (Green 1986; Gallagher and Brown 1997). A trend of post-rift cooling starts around 100 Ma, while a possible second cooling trend could start around 70 Ma; (b) Plot of AFT and AHe ages against elevation. No clear linear trend can be observed before elevations of 1200 m. (For interpretation of the references to colour in this figure legend, the reader is referred to the Web version of this article.)

mean Dpar value, the second highest being sample J-45, with 3.60 µm. The highest obtained Cl wt% value 0.06 was for sample JG-16. Sample JG-17, though with relatively high mean Dpar (3.59 µm), has very low mean Cl wt% (0.017).

Single apatite grains show ages with no statistically significant dispersion and all samples passed the χ^2 test, with unimodal single grain age distributions, with the exception of RJ-36, which has Pχ^2 of 0.6. AFT radial plots and confined track length distributions are presented in the Supplementary Material.

4.2. Apatite U–Th/He data

Mean F_T-corrected ages (Farley et al., 1996) vary between 92.0 ± 11 and 72.9 ± 8.2 Ma and mean AHe raw ages range from 68.1 ± 5.9 to 60.2 ± 7.3 Ma (Table 2). While six single grains were analysed per sample, two grains in sample JG-26 were excluded due to over-dispersed ages. Similarly, grain 3 in sample RJ-37 could not be dated since it was lost from its platinum tube. Single-crystal ages vary between 74.9 ± 5.2 and 48.5 ± 3.4 Ma. All samples show uncorrected ages younger than corresponding AFT ages. Corrected ages are, in turn, younger than their respective AFT ages, with the exception of sample JG-26. However, AFT and AHe corrected age for this sample are within error level of each other.

Although the AHe dataset does not yield significant age dispersion (>20% 1σ standard deviation, Flowers and Kelley, 2011), within-sample age dispersion can be real and contain useful thermal history information whereby age variation is due to variation in grain size (Farley, 2000; Stockli et al., 2000; Reiners and Farley, 2001), composition (Gautheron et al., 2013) and/or radiation damage (Fitzgerald et al., 2006; Shuster et al., 2006; Recanati et al., 2017) as a function of the ^{4}He production during a given thermal history. Alternatively, it might be caused by analytical factors such as unrecognized U–Th-rich inclusion (Lippolt et al., 1994; Farley, 2002), U and Th zonation (Farley, 2002; Meesters and Dunai, 2002a, 2002b; Hourigan et al., 2005; Ault and Flowers, 2012), implantation from U–Th-rich neighbours (Spiegel et al., 2009; Murray and OrmeReiners, 2014), or the analysis of crystal fragments (Brown et al., 2013). The last was avoided by selecting whole grains. For sample JG-26 in particular, there is a weak positive correlation between age and spherical equivalent radius (Fig. 4), which could be a factor indicating F_T overcorrection. Furthermore, thorough grain selection procedures should have reduced the effect of grain zonation and inclusion, while implantation from neighbouring minerals cannot be ruled out. Radiation damage can be assessed through the variation in effective uranium (eU, calculated as [U] + 0.235[Th], Gastil et al., 1967), for which sample JG-26 shows a weak negative correlation with AHe age (Fig. 4), whereas a weak positive correlation could imply radiation damage for sample JG-01. In general, crystal size is varied with spherical equivalent radius (R*) between 44.7 and 107.25 µm, and eU values lie between 16.9 and 57.8 ppm. Samples lack significant correlation between R* or eU and the AHe ages, with the exception of RJ-37, which shows strong positive age-R* correlation (Fig. 4). The AHe data can be further assessed with inverse thermal history models by pairing with the AFT data.

4.3. Inverse thermal modelling

In general, thermal history models show simple, steady cooling trajectories for samples located towards the coast. On the other hand, more complex cooling histories can be seen in areas sampled on the escarpment area or further towards the continental interior. There is not, however, a clear distribution trend between 'simple' and 'complex' models regarding proximity to the coast (Fig. 5). Time-temperature paths shown here are the expected models, which are the mean thermal history model weighed for its posterior probability. Complete models for all samples are available in the Supplementary Material.

The steady cooling models show an onset of cooling mostly between 120 and 100 Ma with an average cooling rate of 0.95 °C/Ma, whereas for the complex models the onset of cooling ranges between 125 and 80 Ma. The latter bear higher cooling rates during the Late Cretaceous (the highest for sample JG-26, 3.6 °C/Ma) followed by a decrease in the cooling rate chiefly between 70 and 50 Ma, with an average cooling rate of 0.34 °C/Ma before reaching surface temperatures. Samples JG-01, RJ-25, JG-26, and RJ-37 show a slight reheating trend then, before reaching surface temperatures. However, temperature increase takes place outside of either AFT PAZ and AHe PRZ (for samples modelled with AHe data - JG-01, JG-26, and RJ-37) and are, as such, poorly resolved.

Estimations of magnitudes of denudation for the modelled samples were calculated as a ratio between the cooling trend temperature variation and the geothermal gradient (Raab et al., 2002), assumed constant at 25 °C/km. This refers to the regionally-averaged mean value of the thermal gradients calculated different sectors of the upper crust in the study area (Hamza et al., 2005a,b; Lima Gomes and Hamza, 2005). Total magnitudes of denudation for that thermal gradient range between 4.5 and 2.5 km. For the regional thermal gradient interval (20–30 °C/km) denudation values range between 5.65-3.15 and 3.77–2.1 km, respectively. Younger AFT ages, towards the coast, reflect high of erosion rates of the South Atlantic Rift flank, and the more complex thermal history models for samples relate to lower magnitudes of denudation towards

Table 2
Summary of results for Apatite U–Th/He analysis.

Sample	Aliquot	^{4}He (ncc)	Mass (mg)	U (ppm)	Th (ppm)	Sm (ppm)	Th/U ratio	L (μm)	W (μm)	R^e (μm)	FT	Raw Age (Ma)	Corrected[a] Age (Ma)	[eU] (ppm)	Raw Age (Ma)		Corrected Age (Ma)	
															Average	SD	Average	SD
JG-01	1	5.7314	0.0199	24.8	41.8	216.2	1.69	298.3	164.0	96.4	0.83	67.5	80.3	34.6	60.2	7.3	72.9	8.2
	2	2.4255	0.0108	25.5	28.0	327.5	1.10	275.4	125.8	76.8	0.78	56.5	70.5	32.1				
	3	3.0366	0.0156	21.3	24.0	253.3	1.13	280.5	149.5	88.5	0.81	58.6	70.8	26.9				
	4	4.1763	0.0174	24.9	26.3	336.6	1.06	313.4	149.4	90.5	0.81	62.5	75.1	31.1				
	5	2.4286	0.0138	24.7	19.3	338.3	0.78	270.1	143.6	85.1	0.80	48.5	59.0	29.2				
	6	7.2922	0.0193	31.2	59.3	401.8	1.90	348.5	149.3	92.2	0.82	67.8	81.5	45.1				
JG-26	1	0.8858	0.0040	21.71	9.04	124.71	0.42	169.0	97.9	56.9	0.70	74.9	101.7	23.8	64.0	8.6	92.0	11.0
	2	0.3060	0.0023	14.29	11.13	58.50	0.78	129.2	85.1	48.0	0.65	63.4	92.6	16.9				
	3	0.6056	0.0035	19.03	29.60	208.29	1.56	201.5	83.8	52.0	0.68	53.8	76.3	26.0				
	4	0.3509	0.0019	19.64	16.66	94.50	0.85	123.1	78.6	44.7	0.62	64.2	97.2	23.6				
JG-37	1	10.3538	0.0276	29.04	50.82	38.33	1.75	338.3	181.3	107.2	0.84	74.8	87.3	41.0	68.1	5.9	81.6	5.4
	2	5.6901	0.0157	33.72	44.83	62.42	1.33	268.7	153.2	89.4	0.81	67.0	80.9	44.3				
	4	4.9315	0.0117	44.25	57.64	50.46	1.30	252.6	136.6	80.6	0.79	59.6	73.5	57.8				
	5	11.8001	0.0240	38.17	72.60	49.88	1.90	347.4	166.9	100.9	0.83	72.7	85.8	55.2				
	6	4.4998	0.0160	23.82	45.27	53.30	1.90	293.2	148.4	88.8	0.81	66.5	80.6	34.5				

Aliquot refers to single grain ages measured in a given sample; L is grain length; W is grain width; R^e is the spherical equivalent radius calculated using the formula $R^e = (3(RL))/(2(R + L))$ where R is the measured radius of the apatite crystal (W/2) and L is the measured length of the apatite crystal; FT is the correction factor after Farley et al. (1996), assuming homogeneous distribution U and Th; eU (effective uranium) is calculated as FT = [eUppm] = [Uppm]+(0.235[Thppm]). a: Corrected AHe age = Raw AHe age/FT.

the continental interior.

Fig. 6 shows thermal history models obtained for samples JG-01, JG-26 and RJ-37, comparing cooling trajectories modelled with AFT data to those modelled with both AFT and AHe data. AFT model for sample JG-26 infers rapid cooling in the Early Cretaceous, followed by a protracted cooling trajectory from the ca. 75 Ma, and a new cooling trend around 20 Ma. The AFT and AHe model, however, presents an earlier onset of cooling and a higher cooling rate, with mild reheating after ca. 90 Ma. Models for samples JG-01 and RJ-37, on the other hand, show considerable change between the cooling curves, from a monotonic cooling trajectory for AFT data alone, to accelerated Early Cretaceous cooling and slower exhumation around 60 Ma. For all AHe thermal history models the expected cooling curve remains in temperatures below the resolution of the method (around 30 °C), while the 95% credible interval is within the upper section of the PRZ during the final cooling phase in samples JG-01 and RJ-37. For all AHe + AFT models the main inferred cooling phase takes place during the Cretaceous, with a later onset of cooling for sample JG-01, on the modern shoreline.

5. Discussion

5.1. Cooling history

Age data and thermal history models indicate a main cooling phase during the Late Cretaceous from temperatures higher than the apatite closing temperatures, with no pre-rift thermal age records for the Precambrian basement. As all samples yield post-rift ages, they were interpreted as cooling ages that reflect basement exhumation from depth. The relationship between AFT ages and MTL shows a clear post-rift cooling event with a boomerang plot (Green, 1986). An initial decrease in track lengths from oldest central ages is followed by an increase in MTL for successively younger ages. A second trend could suggest a new cooling event around 70 Ma, possibly as a consequence of post-rift tectonic activity (Fig. 3a). There is no defined linear relationship between AFT ages and elevation other than for samples above 1200 m.a.s.l., where ages clearly increase with higher altitude (Fig. 3b). Although the onset of exhumation is not constrained by the data, cooling in the Early Cretaceous is likely to have occurred as a response to syn-to post-rift unloading due to denudation. The rapid initial cooling inferred by some of the complex models is mostly seen in the samples currently at high elevations or very close to the coast (e.g. JG-01, J44, RJ-25, JG-26). Accordingly, most of those samples, collected at high-relief locations, yield relatively older ages, narrower track length distributions and longer mean track lengths. While those samples yield older central ages, samples RJ-36 and RJ-37, further inland, show AFT central ages of 91.3 ± 4.7 and 95 ± 3.6 Ma, respectively, at considerably lower elevations. For that group of samples (Fig. 5a) cooling becomes slower during the Late Cretaceous with significantly lower exhumation rates, implying that most of them have resided at near-surface temperatures since then. Samples JG-01 and RJ-25 indicate a third cooling phase in the Neogene, which is not well constrained since cooling trends are outside the limit of resolution for both AFT (for RJ-25) and AHe (for JG-01). Conversely, the other thermal model group (Fig. 5b) presents a single cooling trend since the Early Cretaceous. Groups of samples with similar cooling trajectories (green and blue sample groups for “complex” (a) and “simple” (b) models, respectively, on the topographic profile in Fig. 5) also seem to have a contiguous distribution along certain stretches of the transect, suggesting that localised similar thermal evolutions are a reflection of distinct fault-bounded blocks throughout the transect. For example, the 15-km profile segment on the escarpment with complex thermal models (green) would be a different block from the 10-km segment with simple cooling trajectories (blue). Those blocks would also be limited by a less discernible structural framework (and not only the main structures presented in Fig. 5), which is less evident with the observation of the thermal age data alone.

Total magnitudes of denudation derived for the area are compatible

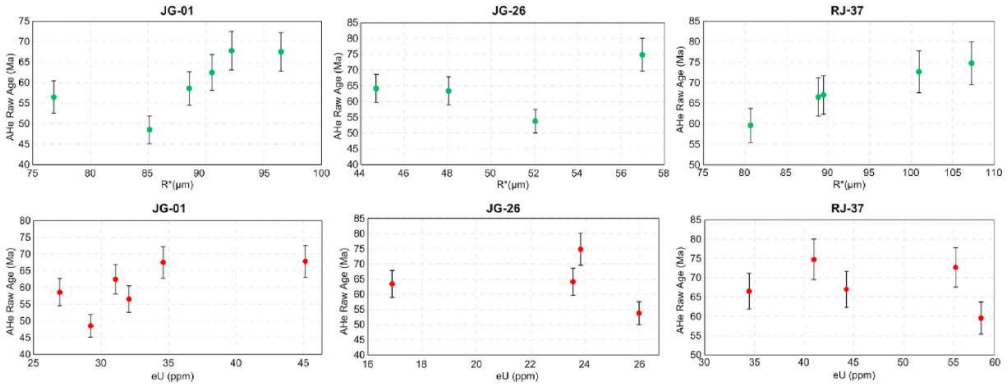

Fig. 4. Plots showing the relationship between single-crystal AHe age and spherical equivalent radius (R*), and effective Uranium (eU), respectively. AHe ages are single grain ages uncorrected for α-ejection.

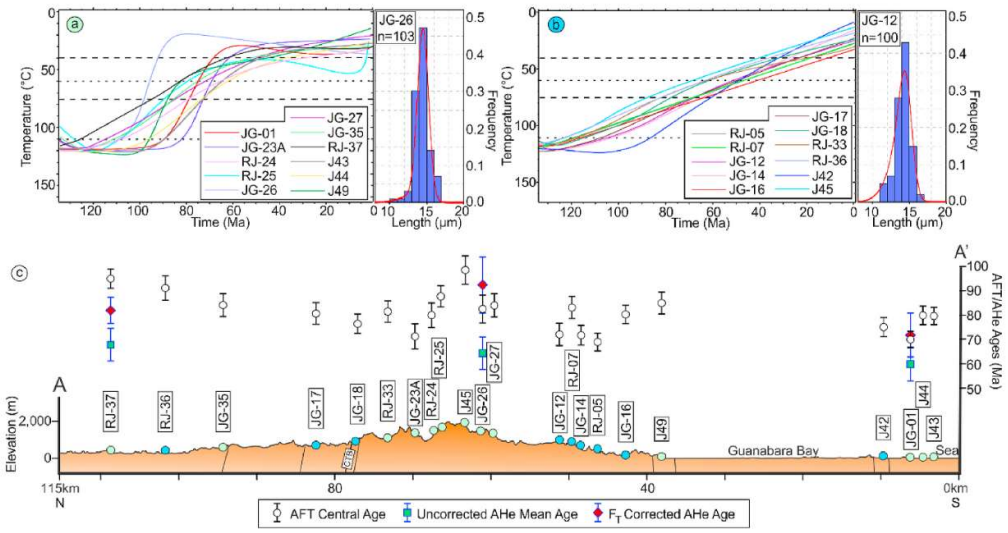

Fig. 5. Expected cooling trajectories for modelled samples with representative track length distributions. Models are divided into (a) complex models, mostly found towards the continental interior and (b) simple models, mostly found for samples closer to the coast, as represented on (c) showing representative topographic profiles with modelled sample locations coloured in reference to model trajectory (green for complex models and blue for simple models) with respective AFT and AHe ages. Schematic main structure position and profile location as shown in Fig. 2. Structure attitude as in Heilbron et al. (2008) and CPRM (2009a,b). CTB is the Central Tectonic Boundary. Thin dashed lines indicate upper and lower limits of apatite FT partial annealing zone (PAZ), while long dash lines indicate those of HePRZ for Durango standard kinetics. (For interpretation of the references to colour in this figure legend, the reader is referred to the Web version of this article.)

with estimates from other studies (Gallagher et al., 1994; Cogné et al. 2011, 2012; Hiruma et al., 2010; Engelmann de Oliveira et al., 2016) for adjacent areas in the SE margin, between ~2 and 4 km, with higher rates of exhumation found for areas closer to the coast. Those values are consistent with sediment thicknesses observed for Late Cretaceous - Paleogene clastic deposits of the proximal Santos and Juréia formations in the Santos Basin, possibly with an important contribution to sand-rich turbiditic deposits in more distal portions of the basins (Zalán and Oliveira, 2005; Assine et al., 2008). A constant geothermal gradient of 25 °C/km is assumed over geological time in the absence of paleo-geothermal data, although it is likely that gradients would be higher during and soon after rifting. Early rapid cooling inferred for complex thermal history models and consequent localised higher denudation rates are also consistent with high rates of sediment supply and basin subsidence observed for the Santos Basin by Contreras et al. (2010). In contrast, Campanian-Maastrichtian decrease in denudation rates for those sites, more common on the escarpment area, coincides with a reduction in the sedimentation rate (Cobbold et al., 2001; Contreras et al., 2010).

5.2. Margin evolution

Thermochronological studies carried out on the southeastern Brazilian continental margin have estimated significant denudation after breakup, between 2.5 and 4 km. Generally, fission-track ages become older towards the interior of the continental margin while younger ages (and respective greater depths of denudation) occur towards the coast. The distinct thermal age ranges found by the authors have been attributed to cooling phases resulting from different phenomena, from studies often combining thermochronological dating to additional radiometric methods. Gallagher et al. (1994), in the most comprehensive regional study regarding the post-rift thermal evolution of the SE continental margin in Brazil to date, noticed denudation and exhumation did not occur at constant rates throughout the margin, as higher average rates were seen towards the coast, with more than 3 km of post-breakup total magnitudes of denudation. The authors found higher complexity in northern and central regions, likely due to structural reactivation. Hackspacher et al. (2004, 2007) suggested tectonic uplift and isostatic movement followed by regional erosive processes as a major mechanism

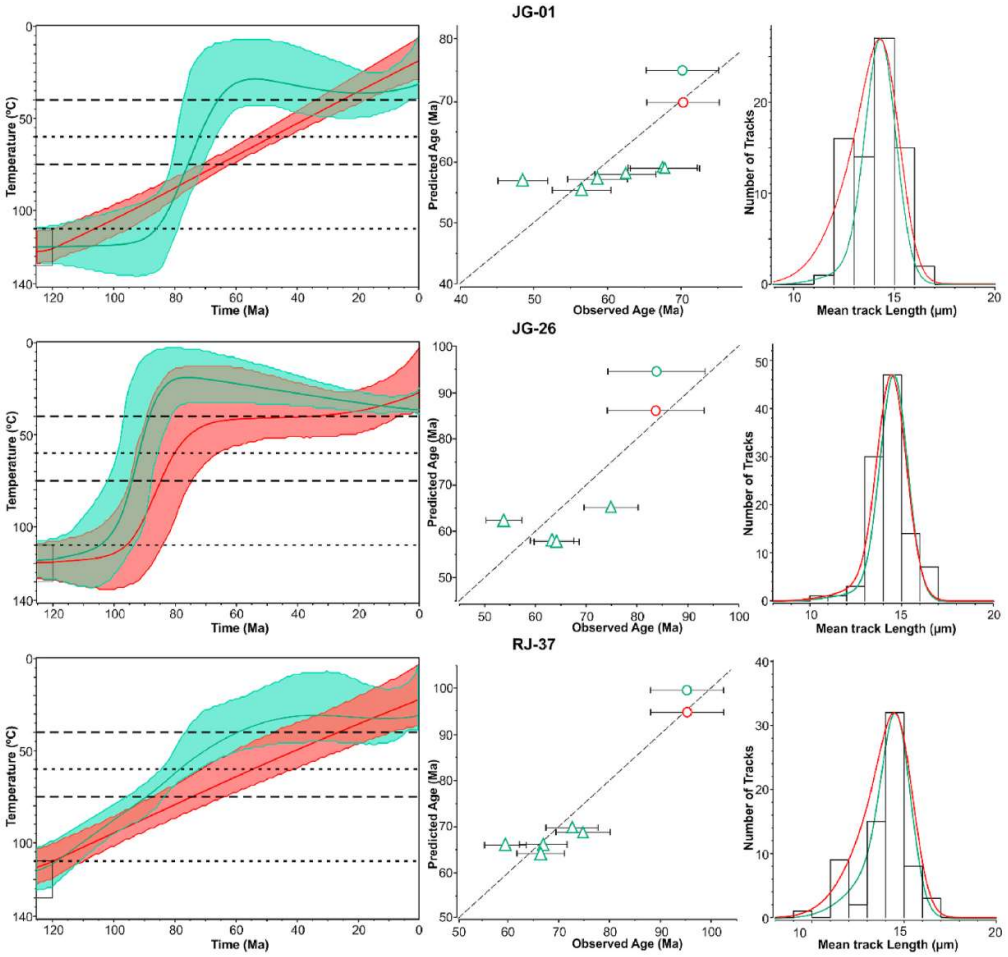

Fig. 6. Cooling history models obtained for coupled AFT and AHe data. For sample thermal history models, on the left, central solid line is the expected model with 95% credible interval. Thin dashed lines indicate upper and lower limits of AFT Partial Annealing Zone (PAZ), and long dash lines indicate those of AHe Partial Retention Zone (PRZ). Central graphs show model age predictions versus observed (measured) ages. Green symbols are for combined AFT and AHe models, while red symbols are for AFT models. Triangles are for AHe ages, and circles are for AFT central ages. Right side graphs present c-axis-projected confined track length distributions for those samples with expected prediction models for each thermal model in its respective colour. (For interpretation of the references to colour in this figure legend, the reader is referred to the Web version of this article.)

for post-rift thermal events. Hiruma et al. (2010) proposed distinct cooling histories locally controlled by fault-bounded blocks in the Bocaina Plateau. Similarly, Karl et al. (2013) and Krob et al. (2019) constrained different crustal blocks for the southeastern and southern segments of the continental margin with different exhumation and cooling histories in multi-thermochonometer studies, recognizing fault-bounded block cooling age control by the Neoproterozoic NE-SW structures as well as by the Atlantic rift transfer zones. Cogné et al. (2011, 2012) and Tello et al. (2003, 2005) described a Neogene uplift in the Serra da Mantiqueira and Serra do Mar escarpments in the state of São Paulo within otherwise distinct thermal history trajectories, which was also identified by Engelmann de Oliveira et al. (2016) for samples in the Paraná Basin and on the Além Paraíba Shear Zone, and attributed its post-rift localized rapid uplift to plate-wide E-W compressional tectonism and structural reactivation as a consequence of Late Cretaceous South America western margin collisions. Franco-Magalhaes et al. (2010) found Late-Cretaceous reactivation of the upper crust, with the youngest AFT ages in the region, reflecting the intrusion of the Ponta Grossa dyke swarm. The thermal history models of samples in this study do not have the resolution to confirm changes in cooling rate in the Neogene.

Gallagher et al. (1994) mention considerable age increase for the AFT ages within 50 km of the present-day coastline. In the present study, however, even though the occurrence of relatively older ages increases towards the continent interior, the age difference is not as pronounced, with the total AFT central age amplitude of the data set of 44.4 ± 5.3 Ma. For example, sample JG-38, collected the farthest inland, has a central age of 68.1 ± 5.1 Ma, some 110 km from the coast. In that sense, the AFT age variability in the area is much lower in compared to other studies in neighbouring areas (Fig. 7).

Engelmann de Oliveira et al. (2016) found similar AFT ages and thermal history models for a basement sample dataset in Rio de Janeiro near this study area. Samples TR7RJ5, TR7RJ6 and TR7RJ7 show cooling ages compatible with those in this study, with AFT central ages ranging between 101.8 ± 6.6 and 73.1 ± 5.5 Ma. The remaining ones, modelled together, exhibit a single, steady cooling trajectory, much like the cooling histories found for the simpler models in the present dataset. Different samples collected along the Além Paraíba Shear Zone on the northern coast, which overlaps the northernmost portion of this study area (Fig. 7), yield younger AFT central ages (between 67.5 ± 5.2 and 48.0 ± 2.9 Ma) and show a steep cooling trend around 4 Ma, which could suggest younger relative structural movement. Sample RJ-35, within 1.5-km distance of the shear zone, doesn't show record of such a process, much like sample RJ-36, which seems to be in line with

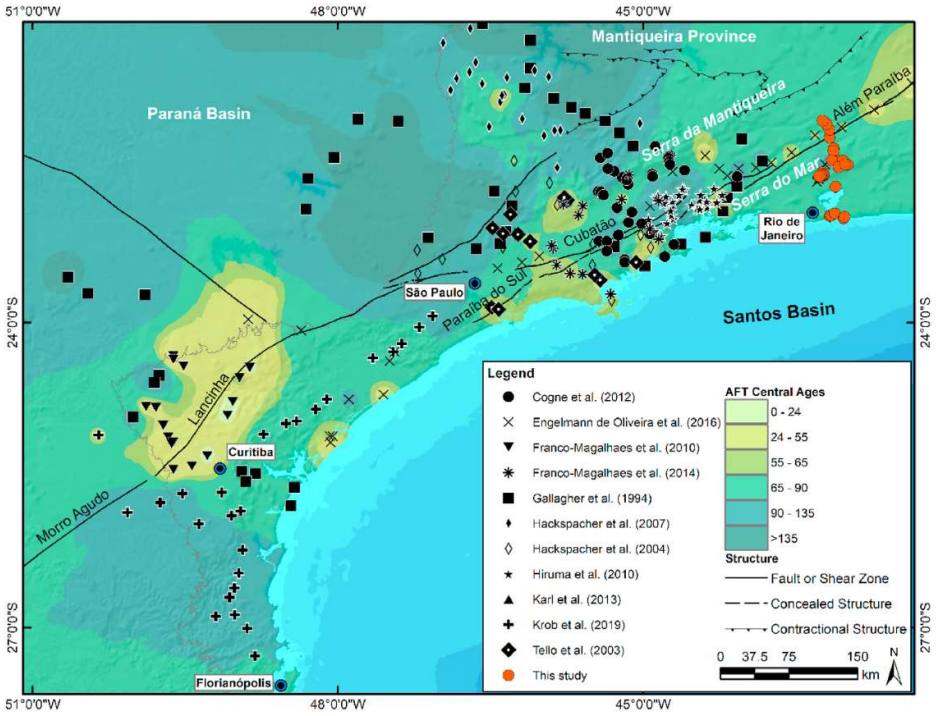

Fig. 7. Location and AFT central age distribution studies throughout the SE segment of the Brazilian continental margin. Younger ages occur towards the coast and in the proximity of large geological structures, implying localised reactivation, whereas older ages are common towards the continental interior and at high elevation features. Central age isolines were plotted using the weighted distance average interpolation tool in software ArcGis 10.5 (ESRI, 2016).

Engelmann de Oliveira et al. (2016)'s samples TR11RJ3 and TR11RJ4.

Post-breakup monotonic cooling is reported for other areas in the SE margin with AFT data models (Cogné et al., 2011; Engelmann de Oliveira et al., 2016), although often for a single sample location or a restricted sector. Likewise, the distribution of steady-cooling models in the study area occurs in segments of the transect, similar to the regional pattern.

Cobbold et al. (2001), Riccomini et al. (2004), and Cogné et al. (2012, 2013) found structural evidence of deformation in the Cenozoic Rift System while evidence of post-rift onshore crustal reactivation was observed in the thermal data for the SE margin, especially in the Paraíba do Sul River Valley (Tello et al. 2003, 2005; Cogné et al. 2011, 2012; Franco-Magalhaes et al., 2014; Engelmann de Oliveira et al., 2016). In the Rio de Janeiro area Ferrari (2001) describes a Campanian - early Eocene E-W transcurrent event responsible for the reactivation of Ribeira Belt structures and formation of the Guanabara Graben (Zalán and Oliveira, 2005). Silicified tectonic breccias in fault zones formed from hydrothermal activity attributed to late-stage alkaline magmatism in the Guanabara Graben have an alkali-feldspar K–Ar age of 50.7 ± 1.2 Ma (Dos Santos, 1994). The youngest AFT age in this study is for sample JG-02 of 54.1 ± 4.2 Ma and was collected from one of the areas where Ferrari (2001) analysed the silicified breccia on the Paineiras Fault (Fig. 2) in the southern area of the city of Rio de Janeiro, on the coast, where the author observed geometric relationships indicating that ENE-WSW reactivation was concomitant with hydrothermal activity. The younger AFT age for sample JG-02 could be related to the reactivation of these structures. Hackspacher et al. (2004) found similar ages in the coastal area in the state of São Paulo (58 ± 4 Ma), which the authors interpreted as an age of reactivation of the Serra do Mar in the area.

The present dataset further illustrates the complexity of the post-rift evolution of the Brazilian continental margin, as numerous factors play different parts in the evolution of distinct segments of the margin. Karl et al. (2013) and Krob et al. (2019) recognized different blocks in the southern SE rifted margin with distinct thermal evolutions since the Brasiliano-Pan-African orogenic cycle, bound by onshore segments of transfer zones. Such sectorisation is likely to be present throughout the margin, controlled by lithospheric heterogeneity and discontinuities (Meisling et al., 2001; Gallagher et al., 1994; Wildman et al., 2019; Hueck et al., 2019). Even though regional high-elevation features share a common post-breakup origin, different segments of the SE margin evolved in a distinct fashion, influenced by particular combinations of mechanisms, as illustrated by the variability amongst available thermochronological datasets. In that sense, we present an indication that the Rio de Janeiro section of the southeastern Brazilian continental margin could have behaved as a distinct block. The sampled area presents relatively uniform exhumation, behaving in a moderately stable manner throughout the post-breakup evolution of the crustal block, in contrast with the more complex trends seen in neighbouring areas.

6. Conclusions

New AFT and AHe thermal data for the state of Rio de Janeiro provide new constraints on the post-breakup evolution of the southeastern segment of the Brazilian continental margin, while highlighting the diversity of processes responsible for the formation of present-day landscape. Sample thermal histories record continuous cooling from as early as the Barremian, associated with rift flank uplift and denudation. Maximum denudation since then is between 2.5 and 4.5 km with greater depths of erosion occurring towards the coastal area. Such volumes are compatible with the high sediment input recorded for the offshore basins, while the Campanian-Maastrichtian decrease in cooling rates observed for samples with more complex cooling histories matches a period of lower sedimentary budget. The relatively uniform distribution of apatite ages across the study area yields little significant variation between high and low elevation areas, in contrast with adjacent studied areas that show more complexity. This contrast points to an important control of the inherited structural framework over the post-breakup

evolution of the rifted margin, as corroborated by other thermochronological studies.

CRediT authorship contribution statement

J.N. Gezatt: Formal analysis, Data curation, Writing - original draft, Visualization, Project administration. **D.I.M. Macdonald:** Visualization, Conceptualization, Supervision. **R. Stephenson:** Writing - review & editing, Visualization, Conceptualization, Supervision. **A.R. Jelinek:** Writing - review & editing, Visualization, Conceptualization, Supervision. **A. Carter:** Formal analysis, Data curation, Writing - review & editing, Visualization.

Declaration of competing interest

The authors declare that they have no known competing financial interests or personal relationships that could have appeared to influence the work reported in this paper.

Acknowledgements

We gratefully acknowledge support from Shell Brazil through the BG05: UoA-UFRGS-SWB Sedimentary Systems project at the University of Aberdeen and UFRGS, and the strategic importance of the support given by ANP through the RandD levy regulation. Conselho Nacional de Desenvolvimento Científico e Tecnológico (CNPq) process number 237726/2012-2 for funding under regime GDE of the Science Without Borders Programme. We would also like to thank the London Geochronology Centre for access to their analytical facilities, welcome and assistance. We are grateful to Kerry Gallagher for the advice on the thermal modelling, and to Mark Wildman for the discussions. Finally, we thank the two reviewers for their constructive suggestions that have led to improvements in the final version of the manuscript.

Appendix A. Supplementary data

Supplementary data to this article can be found online at https://doi.org/10.1016/j.jsames.2020.103051.

References

Almeida, F.F.M., 1991. O alinhamento magmatico de Cabo Frio, 2°. Simpósio de Geologia do Sudeste, São Paulo, pp. 423–428.
Almeida, F.F.M., Carneiro, C.D.R., Mizusaki, A.M.P., 1996. Correlação do magmatismo dasBacias da Margem Continental Brasileira com o das áreas emersas adjacentes. Revista Brasileira de Geosciências. v. 23 (3), 125–138.
Aslanian, D., Moulin, M., Olivet, J.L., Unternehr, P., Matias, L., Bache, F., Rabineau, M., Nouzé, H., Klingelhoefer, F., Contrucci, I., Labails, C., 2009. Brazilian and african passive margins of the central segment of the south Atlantic Ocean: kinematic constraints. Tectonophysics 468, 98–112.
Assine, M.L., Corrêa, F.S., Chang, H.K., 2008. Migração de depocentros na Bacia de Santos: importância na exploração de hidrocarbonetos. Rev. Bras. Geociencias 38 (2), 111–127.
Ault, A.K., Flowers, R., 2012. Is apatite U–Th zonation information necessary for accurate interpretation of apatite (U–Th)/He thermochronometry data? Geochem. Cosmochim. Acta 79, 60–78.
Ault, A.K., Gautheron, C., King, G.E., 2019. Innovations in (U–Th)/He,fission track, and trapped charge thermochronometry with applications to earthquakes, weathering, surface-mantle connections, and the growth and decay of mountains. Tectonics 38, 3705–3739.
Beglinger, S.E., Doust, H., Cloetingh, S., 2012. Relating petroleum system and play development to basin evolution: Brazilian South Atlantic margin. Petrol. Geosci. 18, 315–336.
Blenkinsop, T., Moore, A., 2013. Tectonic geomorphology of passive margins and continental hinterlands. In: Owen, L.A., Shroder, J.F. (Eds.), Treatise on Geomorphology 5. Academic Press, San Diego, pp. 71–92.
Brito Neves, B.B., Cordani, U.G., 1991. Tectonic evolution of South America during the late proterozoic. Precambrian Res. 53, 23–40.
Brito Neves, B.B., Fuck, R.A., Pimentel, M.M., 2014. The Brasiliano collage in South America: a review. Braz. J. Genet. 44 (3), 493–518.
Brown, R.W., Rust, D.J., Summerfield, M.A., Gleadow, A.J., De Wit, M.C., 1990. An Early Cretaceous phase of accelerated erosion on the south-western margin of Africa: evidence from apatite fission track analysis and the offshore sedimentary record. Int. J. Radiat. Appl. Instrum. Nucl. Tracks Radiat. Meas. 17 (3), 339–350.
Brown, R.W., Summerfield, M.A., Gleadow, A.J.W., 2002. Denudational history along transect across the Drakensberg Escarpment of southern Africa derived from apatite fission track thermochronology. J. Geophys. Res. 107, 23–50.
Brown, R.W., Beucher, R., Roper, S., Persano, C., Stuart, F., Fitzgerald, P., 2013. Natural age dispersion arising from the analysis of broken crystals. Part I: theoretical basis and implications for the apatite (U–Th)/He thermochronometer. Geochem. Cosmochim. Acta 122, 478–497.
Brune, S., Williams, S.E., Müller, R.D., 2018. Oblique rifting: the rule, not the exception. Solid Earth 9, 1187–1206.
Buiter, S.J.H., Torsvik, T.H., 2014. A review of Wilson Cycle plate margins: a role for mantle plumes in continental break-up along sutures? Gondwana Res. 26 (2), 627–653.
Chang, H.K., Kowsmann, R.O., Figueiredo, A.M.F., Bender, A.A., 1992. Tectonics and stratigraphy of the East Brazil Rift system: an overview. Tectonophysics 213, 97–138.
Cainelli, C., Mohriak, W.U., 1999. Some remarks on the evolution of sedimentary basins along the eastern Brazilian continental margin. Episodes 22 (3), 206–216.
Cobbold, P.R., Meisling, K.E., Mount, V.S., 2001. Reactivation of an obliquely rifted margin, Campos and Santos basins, southeastern Brazil. AAPG (Am. Assoc. Pet. Geol.) Bull. 85, 1925–1944.
Cogné, N., Gallagher, K., Cobbold, P.R., 2011. Post-rift reactivation of the onshore margin of southeast Brazil: evidence from apatite (U–Th)/He and fission-track data. Earth Planet Sci. Lett. 309, 118–130. Issues 1–2.
Cogné, N., Gallagher, K., Cobbold, P.R., Riccomini, C., Gautheron, C., 2012. Post-breakup tectonics in southeast Brazil from thermochronological data and combined inverse forward thermal history modeling. J. Geophys. Res. 117, B11413.
Cogné, N., Cobbold, P.R., Riccomini, C., 2013. Tectonic setting of the Taubaté Basin (Southeastern Brazil): insights from regional seismic profiles and outcrop data. J. S. Am. Earth Sci. 42, 194–204.
Contreras, J., Zühlke, R., Bowman, S., Bechstädt, T., 2010. Seismic stratigraphy and subsidence analysis of the southern Brazilian margin (Campos, Santos and Pelotas basins). Mar. Petrol. Geol. 27, 1952–1980.
CPRM, 2009a. Mapa geológico. Folha baía de Guanabara. Rio de Janeiro, RJ. SF23-Z-B-IV. Scale: 1:100,000.
CPRM, 2009b. Mapa geológico. Folha de Três Rios. Rio de Janeiro, RJ. SF23-Z-B-I. Scale: 1:100,000.
Donelick, R.A., O'Sullivan, P.B., Ketcham, R.A., 2005. Apatite fission-track analysis. Rev. Mineral. Geochem. 58 (1), 49–94.
Dos Santos, R.P., 1994. Datation K/Ar et Rb/Sr d'argiles de minéralisations et de diagenèse le long de la côte Est de l'Amérique du Sud: implications géodynamiques. PhD Thesis. Université Joseph-Fourier - Grenoble I, p. 267.
Ebert, H.D., Hasui, Y., 1998. Transpressional tectonics and strain partitioning during oblique collision between three plates in the Precambrian of south-east Brazil. In: Holdsworth, R.E., Strachan, R.A., Dewey, J.E.((Eds.), Continental Transpressional and Transtensional Tectonics, vol. 135. Geological Society, London, Special Publications, pp. 231–252.
Engelmann de Oliveira, C.H.E., Jelinek, A.R., Chemale Jr., F., Cupertino, J.A., 2016. Thermotectonic history of the southeastern Brazilian margin: evidence from apatite fission track data of the offshore Santos Basin and continental basement. Tectonophysics 685, 21–34.
ESRI, 2016. ArcGIS Desktop: Release 10.5. Environmental Systems Research Institute, Redlands, CA.
Farley, K.A., 2000. Helium diffusion from apatite: general behaviour as illustrated by Durango fluorapatite. J. Geophys. Res. 105, 2903–2914.
Farley, K.A., 2002. U-Th)/He dating: techniques, calibrations, and applications. Rev. Mineral. Geochem. 47 (1), 819–844.
Farley, K.A., Wolf, R.A., Silver, L.T., 1996. The effects of long alpha-stopping distances on (U-Th)/He ages. Geochem. Cosmochim. Acta 60 (21), 4223–4229.
Ferrari, A.L., 2001. Evolução tectônica do Gráben da Guanabara. PhD Thesis. University of São Paulo.
Fitzgerald, P.G., Baldwin, S.L., Webb, L.E., O'sullivan, P.B., 2006. Interpretation of (U–Th)/He single grain ages from slowly cooled crustal terranes: a case study from the Transantarctic Mountains of southern Victoria Land. Chem. Geol. 225 (1), 91–120.
Flowers, R.M., Ketcham, R.A., Shuster, D.L., Farley, K.A., 2009. Apatite (U–Th)/He thermochronometry using a radiation damage accumulation and annealing model. Geochem. Cosmochim. Acta 73 (8), 2347–2365.
Flowers, R.M., Kelley, S.A., 2011. Interpreting data dispersion and "inverted" dates in apatite(U–Th)/He and fission-track datasets: an example from the US midcontinent. Geochem. Cosmochim. Acta 75, 5169–5186.
Franco-Magalhaes, A.O.B., Hackspacher, P.C., Glasmacher, U.A., Saad, A.R., 2010. Rift to post-rift evolution of a "passive" continental margin: the Ponta Grossa Arch, SE Brazil. Int. J. Earth Sci. 99, 1599–1613.
Franco-Magalhaes, A.O.B., Cuglieri, M.A.A., Hackspacher, P.C., Saad, A.R., 2014. Long-term landscape evolution and post-rift reactivation in the southeastern Brazilian passive continental margin: taubaté basin. Int. J. Earth Sci. 103, 441–453.
Galbraith, R.F., 1992. Statistical models for mixed ages. International Workshop on Fission Track Thermochronology, Philadelphia.
Gallagher, K., 1995. Evolving temperature histories from apatite fission-track data. Earth Planet Sci. Lett. 136, 421–435.
Gallagher, K., 2012. Transdimensional inverse thermal history modelling for quantitative thermochronology. Journal of Physical Research 117, 1–16.
Gallagher, K., Brown, R., 1997. The onshore record of passive margin evolution. J. Geol. Soc. 154 (3), 451–457.

Gallagher, K., Hawkesworth, C.H., Mantovani, M.S.M., 1994. The denudation history of the onshore continental margin of the SE Brazil inferred from apatite fission track data. J. Geophys. Res. 99. B9. p. 18,117 -118,145.
Gastil, R.G., DeLisle, M., Morgan, J., 1967. Some effects of progressive metamorphism on zircons. Geol. Soc. Am. Bull. 78, 879–906.
Gautheron, C., Tassan-Got, L., Barbarand, J., Pagel, M., 2009. Effect of alpha-damage annealing on apatite (U-Th)/He thermochronology. Chem. Geol. 266 (3-4), 157–170.
Gautheron, C., Barbarand, J., Ketcham, R.A., Tassan-Got, L., van der Beek, P.A., Pagel, M., et al., 2013. Chemical influence on α-recoil damage annealing in apatite: implications for (U-Th)/He dating. Chem. Geol. 351, 257–267.
Green, P.F., 1986. On the thermo-tectonic evolution of northern England; evidence from fission track analysis. Geol. Mag. 123, 493–506.
Geraldes, M.C., Motoki, A., Costa, A., Mota, C.E., Mohriak, W.U., 2013. Geochronology (Ar/Ar and K–Ar) of the south atlantic post-break-up magmatism. In: Mohriak, W.U., Danforth, A., Post, P.J., Brown, D.E., Tari, G.C., Nemčok, M., Sinha, S.T. (Eds.), Conjugate Divergent Margins, vol. 369. Geological Society, London, Special Publications, pp. 41–74.
Gilchrist, A., Summerfield, M.A., 1990. Differential denudation and flexural isostasy in formation of rifted-margin upwarps. Nature 346, 739–742.
Gleadow, A.J.W., 1981. Fission-track dating methods: what are the real alternatives? Nucl. Tracks 5, 3–14.
Gleadow, A.J.W., Duddy, I.R., Green, P.F., Lovering, J.F., 1986. Confined fission track lengths in apatite: a diagnostic tool for thermal history analysis. Contrib. Mineral. Petrol. 94 (4), 405–415.
Hackspacher, P.C., Ribeiro, L.F.B., Fetter, A.H., Hadler Neto, J.C., Tello Sáenz, C.E., Dantas, E.L., 2004. Consolidation and break-up of the South American Platform in southeastern Brazil: tectonothermal and denudation histories. Gondwana Res. 7 (1), 91–101.
Hackspacher, P.C., Godoy, D.F., Ribeiro, L.F.B., Hadler, J.C., Franco, A.O.B., 2007. Modelagem térmica e geomorfologia da borda sul do Cráton do São Francisco: termocronologia por traços de fissão em apatita. Rev. Bras. Geociencias 37 (4), 76–86.
Hamza, V.M., Cardoso, R.A., Gomes, A.J.L., 2005a. Gradiente e fluxo geotérmico na região sudeste: indícios de calor residual do magmatismo alcalino e implicações para maturação térmica de sedimentos na plataforma continental. Anais do III Simpósio de Vulcanismo e Ambientes Associados, Cabo Frio, Rio de Janeiro 319–324.
Hamza, V.M., Dias, F.J.S., Gomes, A.J.L., Terceros, Z.G.D., 2005b. Numerical and functional representations of regional heat flow in South America. Phys. Earth Planet. In. 152, 223–256.
Heilbron, M., Valeriano, C.M., Tassinari, C.C.G., Almeida, J., Tupinambá, M., Siga Jr., O., Trouw, R., 2008. Correlation of Neoproterozoic terranes between the Ribeira Belt, SE Brazil and its African counterpart: comparative tectonic evolution and open questions. In: Pankhurst, R.J., Trouw, R.A.J., Brito Neves, B.B., De Wit, M.J. (Eds.), West Gondwana: Pre-cenozoic Correlations across the South Atlantic Region, vol. 294. The Geological Society of London Special Publications, London, pp. 211–237.
Heilbron, M., Silva, L.G.E., Almeida, J.C.H., Tupinambá, M., Peixoto, C., Valeriano, C.M., Lobato, M., Rodrigues, S.W.O., Ragatky, C.D., Silva, M.A., Monteiro, T., Freitas, N.C., Miguens, D., Girão, R., 2020. Proterozoic to Ordovician geology and tectonic evolution of Rio de Janeiro State, SE-Brazil: insights on the central Ribeira Orogen from the new 1:400,000 scale geologic map. Braz. J. Genet. 50 (2), 1–25.
Heine, C., Zoethout, J., Müller, R.D., 2013. Kinematics of the south Atlantic Rift. Solid Earth 4, 215–253.
Hiruma, S.T., Riccomini, C., Modenesi-Gauttieri, M.C., Hackspacher, P.C., Hadler Neto, J.C., Franco-Magalhães, A.O.B., 2010. Denudation history of the Bocaina Plateau, Serra do Mar, southeastern Brazil: relationships to Gondwana breakup and passive margin development. Gondwana Res. 18 (4), 674–687.
Hourigan, J.K., Reiners, P.W., Brandon, M.T., 2005. U–Th zonation-dependent a-ejection in (U–Th)/He chronometry. Geochimica et Cosmochimica Acta. Acta 69, 3349–3365.
Hueck, M., Dunkl, I., Oriolo, S., Wemmer, K., Basei, M.A.S., Siegesmund, S., 2019. Comparing contiguous high- and low-elevation continental margins: new (U-Th)/He constraints from South Brazil and an integration of the thermochronological record of the southeastern passive margin of South America. Tectonophysics 770, 228222.
Hurford, A.J., 1990. Standardization of fission track dating calibration: recommendation by the fission track working group of the I.U.G.S. Subcommission on Geochronology. Chem. Geol. 80, 171–178.
Hurford, A.J., Green, P.F., 1982. A user's guide to fission track dating calibration. Earth Planet Sci. Lett. 59, 343–354.
Janasi, V.A., Freitas, V.A., Heaman, L.H., 2011. The onset of flood basalt volcanism, Northern Paraná Basin, Brazil: a precise U–Pb baddeleyite/zircon age for a Chapecó-type dacite. Earth Planet Sci. Lett. 302, 147–153.
Japsen, P., Chalmers, J.A., Green, P.F., Bonow, J.M., 2012. Elevated, passive continental margins: not rift shoulders, but expressions of episodic, post-rift burial and exhumation. Global Planet. Change 90–91, 73–86.
Jelinek, A.R., Chemale Jr., F., van der Beek, P.A., Guadagnin, F., Cupertinio, J.A., 2014. Denudation history and landscape evolution of the northern East-Brazilian continental margin from apatite fission-track thermochronology. J. S. Am. Earth Sci. 54, 158–181.
Karl, M., Glasmacher, U.A., Kollenz, S., Franco-Magalhães, A.O.B., Stockli, D.F., Hackspacher, P.C., 2013. Evolution of the South Atlantic passive continental margin in southern Brazil derived from zircon and apatite (U-Th-Sm)/He and fission-track data. Tectonophysics 604, 224–244.
Karner, G.D., Driscoll, N.W., 1999. Tectonic and stratigraphic development of the West African and eastern Brazilian Margins: insights from quantitative basin modelling. In: Cameron, N.R., Bate, R.H., Clure, V.S. (Eds.), The Oil and Gas Habitats of the South Atlantic, vol. 153. The Geological Society of London Special Publications, London, pp. 11–40.
Ketcham, R.A., Carter, A., Donelick, R.A., Barbarand, J., Hurford, A.J., 2007. Improved modelling of fission-track annealing in apatite. Am. Mineral. 92 (5–6), 799–810.
Krob, F.C., Glasmacher, U.A., Karl, M., Perner, M., Hackspacher, P.C., Stockli, D.F., 2019. Multi-chronometer thermochronological modelling of the Late Neoproterozoic to recent t-T-evolution of the SE coastal region of Brazil. J. S. Am. Earth Sci. 92, 77–94.
Lima Gomes, A.J., Hamza, V.M., 2005. Geothermal gradient and heat flow in the state of Rio de Janeiro. Rev. Bras. Geofís. 23 (4), 325–347.
Lippolt, H.J., Leitz, M., Wernicke, R.S., Hagedorn, B., 1994. Uranium+thorium)/helium dating of apatite: experience with samples from different geochemical environments. Chemical Geology; Isotope Geoscience 112, 179–191.
Macdonald, D., Gomez-Perez, I., Franzese, J., Spalletti, L., Lawyer, L., Gahagan, L., Dalziel, I., Thomas, C., Trewin, N., Hole, M., Paton, D., 2003. Mesozoic break-up of SW Gondwana: implications for regional hydrocarbon potential of the southern South Atlantic. Mar. Petrol. Geol. 20 (3–4), 287–308.
McGregor, E.D., Nielsen, S.B., Stephenson, R.A., Petersen, K.D., Macdonald, D.I.M., 2013. Long-term exhumation of a Palaeoproterozoic orogen and the role of pre-existing heterogeneous thermal crustal properties: a fission-track study of SE Baffin Island. J. Geol. Soc. 170, 877–891. London.
Meesters, A.G.C.A., Dunai, T.J., 2002a. Solving the production–diffusion equation for finite diffusion domains of various shapes: Part I. Implications for low-temperature (U–Th)/He thermochronology. Chem. Geol. 186 (3), 333–344.
Meesters, A.G.C.A., Dunai, T.J., 2002b. Solving the production–diffusion equation for finite diffusion domains of various shapes: Part II. Application to cases with α-ejection and nonhomogeneous distribution of the source. Chem. Geol. 186 (3), 347–363.
Meisling, K.E., Cobbold, P.R., Mount, V.S., 2001. Segmentation of an obliquely rifted margin, Campos and Santos basins, southeastern Brazil. AAPG Bulletin. v. 85 (11), 1903–1924.
Milani, E.J., Brandão, A.S.L., Zalán, P.V., Gambia, L.A.P., 2001. Petróleo na margem continental brasileira: geologia, exploração, resultados e perspectivas. Braz. J. Genet. 18, 352–396.
Modica, C.J., Brush, E.R., 2004. Postrift sequence stratigraphy, paleogeography, and fill history of the deep-water Santos Basin, offshore southeast Brazil. AAPG (Am. Assoc. Pet. Geol.) Bull. 88, 923–945.
Mohriak, W.U., Hobbs, R., Dewey, J.F., 1990. Basin-forming processes and the deep structure of the Campos Basin, offshore Brazil. Mar. Petrol. Geol. 7 (2), 101–122.
Murray, K.E., Orme, D.A., Reiners, P.W., 2014. Effects of U–Th-rich grain boundary phases on apatite helium ages. Chem. Geol. 390, 135–151.
Nielsen, S.B., Gallagher, K., Leighton, C., Balling, N., Svenningsen, L., Jacobsen, B.H., Thomsen, E., Nielsen, O.B., Heilmann-Clausen, C., Egholm, D.L., Summerfield, M.A., Clausen, O.R., Piotrowski, J.A., Thorsen, M.R., Huuse, M., Abrahamsen, N., King, C., Lykke-Andersen, H., 2009. The evolution of western Scandinavian topography: a review of Neogene uplift versus the ICE (isostasy–climate–erosion) hypothesis. J. Geodyn. 47 (2–3), 72–95.
O'Sullivan, P.B., Mitchell, M.M., O'Sullivan, A.J., Kohn, B.P., Gleadow, A., 2000. Thermotectonic history of the Bassian Rise, Australia: implications for the breakup of eastern Gondwana along Australia's southeastern margins. Earth Planet Sci. Lett. 182, 31–47.
Pichel, L.M., Jackson, C.A., Peel, F., Dooley, T.P., 2019. Base-salt relief controls on salt-tectonic structural style, São Paulo plateau, Santos basin, Brazil. Basin Res. https://doi.org/10.1111/bre.12375.
Raab, M.J., Brown, R.W., Gallagher, K., Carter, A., Weber, K., 2002. Late Cretaceous reactivation of major crustal shear zones in northern Namibia: constraints from apatite fission track analysis. Tectonophysics. v. 349 (1), 75–92.
Recanati, A., Gautheron, C., Barbarand, J., Missenard, Y., Rinna-Jamme, R., Tassan-Got, L., et al., 2017. Helium trapping in apatite damage: insights from (U-Th-Sm)/He dating of different granitoid lithologies. Chem. Geol. 470, 116–131.
Reiners, P.W., Farley, K.A., 2001. Influence of crystal size on apatite (U–Th)/He thermochronology: an example from the Bighorn Mountains, Wyoming. Earth Planet Sci. Lett. 188 (3–4), 413–420.
Riccomini, C., Sant'Anna, L.G., Ferrari, A.L., 2004. Evolução geológica do rift continental do sudeste do brasil. In: Mantesso-Neto, V., Bartorelli, A., Carneiro, C.D.R., Brito-Neves, B.B. (Eds.), Geologia do Continente Sul-Americano: Evolução da Obra de Fernando Flávio Marques de Almeida. Edições Beca, São Paulo, pp. 383–405.
Riccomini, C., Velázquez, V.F., Gomes, C.B., 2005. Tectonic controls of the Mesozoic and Cenozoic alkaline magmatism in central-southeastern Brazilian Platform. In: Gomes, C.B., Comin-Chiaramonti, P. (Eds.), Mesozoic to Cenozoic Alkaline Magmatism in the Brazilian Platform. EDUSP-FAPESP, São Paulo, pp. 31–55.
Sacek, V., Braun, J., van der Beek, P., 2012. The influence of rifting on escarpment migration on high elevation continental margins. J. Geophys. Res. 117, B04407.
Stanton, N., Schimitt, R., Galdeano, A., Maia, M., Mane, M., 2010. Crustal structure of the southeastern Brazilian margin, Campos Basin, from aeromagnetic data: new kinematic constraints. Tectonophysics 490, 15–27.
Schmitt, R.S., Throuw, R.A.J., Van Schmus, W.R., Passchier, C.W., 2008. Cambrian orogeny in the Ribeira Belt (SE Brazil) and correlations within West Gondwana: ties that bind underwater. In: Pankhurst, R.J., Trouw, R.A.J., Brito Neves, B.B., de Wit, M.J. (Eds.), West Gondwana: Pre-cenozoic Correlations across the South Atlantic Region, vol. 294. The Geological Society of London Special Publications, London, pp. 279–296.
Schmitt, R.S., Trouw, R., Van Schmus, W.R., Armstrong, R., Stanton, N.S.G., 2016. The tectonic significance of the Cabo Frio Tectonic Domain in the SE Brazilian margin: a Paleoproterozoic through Cretaceous saga of a reworked continental margin. Braz. J. Genet. 46 (1), 37–66.

Shuster, D.L., Flowers, R.M., Farley, K.A., 2006. The influence of natural radiation damage on helium diffusion kinetics in apatite. Earth Planet Sci. Lett. 249 (3), 148–161.

Spiegel, C., Kohn, B.P., Belton, D., Brener, Z., Gleadow, A.J.W., 2009. Apatite (U–Th–Sm)/He thermochronology of rapidly cooled samples: the effect of He implantation. Earth Planet Sci. Lett. 385, 105–119.

Stica, J.M., Zalán, P.V., Ferrari, A.L., 2014. The evolution of rifting on the volcanic margin of the pelotas Basin and the contextualization of the paranáe etendeka LIP in the separation of Gondwana in the south atlantic. Mar. Petrol. Geol. 50, 1–21.

Stockli, D.F., Farley, K.A., Dumitru, T.A., 2000. Calibration of the apatite (U–Th)/He thermochronometer on an exhumed fault block, White Mountains, California. Geology 28, 983–986.

Tello, S.C.A., Hackspacher, P.C., Hadler Neto, J.C., Iunes, P.J., Guedes, S., Paulo, S.R., Ribeiro, L.F.B., 2003. Recognition of cretaceous, paleocene and Neogene tectonic reactivation, through apatite fission-track analysis, in precambrian areas of the southeast Brazil: association with the south Atlantic Ocean opening. Journal of South American Earth Scieces 15, 137–142.

Tello, S.C.A., Hadler Neto, J.C., Iunes, P.J., Guedes, S., Hackspacher, P.C., Ribeiro, L.F.B., Paulo, S.R., Osório, A.M.A., 2005. Thermochronology of the South American Platform in the state of São Paulo, Brazil, through apatite fission tracks. Radiat. Meas. 39, 635–640.

Thiede, D.S., Vasconcelos, P.M., 2010. Paraná flood basalts: rapid extrusion hypothesis confirmed by new 40Ar/39Ar results. Geology. v. 38 (8), 747–750.

Thomaz Filho, A., Mizusaki, A.M.P., Antonioli, L., 2008. Magmatismo nas bacias sedimentares brasileiras e sua influência na geologia do petróleo. Rev. Bras. Geociencias 38 (2), 128–137.

Thompson, R.N., Gibson, S.A., Mitchell, J.G., Dickin, A.P., Leonardos, O.H., Brod, J.A., Greenwood, J.C., 1998. Migrating cretaceous-eocene magmatism in the Serra do mar alkaline Province, SE Brazil: melts from the deflected trindade mantle plume? J. Petrol. 39, 1493–1526.

Tommasi, A., Vauchez, A., 2001. Continental rifting parallel to ancient collisional belts: an effect of the mechanical anisotropy of the lithospheric mantle. Earth Planet Sci. Lett. 185, 199–210.

Trouw, R.A.J., Heilbron, M., Ribeiro, A., Paciullo, F.V.P., Valeriano, C.M., Almeida, J.C. H., Tupinambá, M., Andreis, R.R., 2000. The central segment of the Ribeira Belt. In: Cordani, U.G., Milani, E.J., Thomaz Filho, A., Campos, D.A. (Eds.), Tectonic Evolution of South America. 31st International Geological Congress, pp. 287–310. Rio de Janeiro.

Vieira, B.C., Gramani, M.F., 2015. Serra do Mar: the most "tormented" relief in Brazil. In: Vieira, B.C., Salgado, A.A.R., Santos, L.J.C. (Eds.), Landscape and Landforms of Brazil. Springer, pp. 285–298.

Wagner, G.A., Gleadow, A.J.W., Fitzgerald, P.G., 1989. The significance of the partial annealing zone in apatite fission-track analysis: projected track length measurements and uplift chronology of the Transantarctic Mountains. Chem. Geol. 79, 295–305.

Wildman, M., Brown, R., Watkins, R., Carter, A., Gleadow, A., Summerfield, M., 2015. Post break-up tectonic inversion across the southwestern cape of South Africa: new insights from apatite and zircon fission track thermochronometry. Tectonophysics 654, 30–55.

Wildman, M., Cogné, N., Beucher, R., 2019. Fission-track thermochronology applied to the evolution of passive continental margins. In: Malusà, M.G., Fitzgerald, P.G. (Eds.), Fission-Track Thermochronology and its Application to Geology. Springer Textbooks in Earth Sciences, Geography and Environment, pp. 351–371.

Zalán, P.V., Oliveira, J.A.B., 2005. Origem e evolução estrutural do Sistema de Riftes Cenozóicos do Sudeste do Brasil. Bol. Geociencias Petrobras 13, 269–300.